Proceedings of the 16th International Workshop on Rare Earth Magnets and their Applications, September 10 - 13, 2000, Sendai, Japan

Microstructure and Hard Magnetic Properties of Cu and Nb Containing Nd-Fe-B Nanocomposites

D. H. Ping, Y. Q. Wu, H. Kanekiyo*, S. Hirosawa* and K. Hono

National Research Institute for Metals, 1-2-1 Sengen, Tsukuba 305-0047, Japan
**Sumitomo Special Metals Co., Ltd., 2-15-17 Egawa, Osaka 618-0013, Japan*

Abstract

This paper reports the effect of Cu and Nb additions on the microstructure and magnetic properties of $Fe_3B/Nd_2Fe_{14}B$ and α-Fe/$Nd_2Fe_{14}B$ nanocomposites. Minor addition of Cu to $Nd_{4.5}Fe_{77}B_{18.5}$ alloy is effective in refining the $Fe_3B/Nd_2Fe_{14}B$ nanocomposite microstructure that are produced by crystallization of amorphous phase. While single addition of Nb show adverse effect on the grain size of the nanocomposite, combined addition of Cu and Nb to $Nd_{4.5}Fe_{77}B_{18.5}$ show beneficial effect on the nanocomposite microstructure and the hard magnetic properties. On the other hand, addition of Cu is not beneficial in refining α-Fe/$Nd_2Fe_{14}B$ nanocomposites. The role of these additives in the microstructural evolution from Nd-Fe-B based amorphous alloys is discussed based on transmission electron microscopy and atom probe analysis results.

Introduction

Optimization of microstructure is the key to improve the hard magnetic properties of the existing nanocomposite magnets. Refinement of the nanocomposite microstructure in less than 20 nm is essential to obtain high coercivity and high energy product. On this bases, many attempts have been made to improve the magnetic properties of nanocomposite magnets by adding quaternary and quinery elements in Fe-Nd-B ternary alloys[1-3]. In softmagnetic Fe-Si-B amorphous alloy, Yoshizawa and Yamauchi [4] reported that additions of Cu and Nb have drastic effect in reducing the grain size of the crystallized nanocrystalline structure. By visualizing the spatial distributions of the alloying elements in Fe-Si-B-Nb-Cu nanocrystalline alloys using atom probe, we revealed that Cu atoms form clusters in the early stage of the crystallization reaction, which serve as heterogeneous nucleation sites for the primary crystals, thereby reducing the grain size of the final microstructure [5]. Since Cu has large positive enthalpy of mixing with Fe, it tends to decompose from the Fe based matrix, forming Cu-enriched clusters. These Cu clusters develop to fcc-Cu, which provide heterogeneous nucleation site for α-Fe primary crystals. If Cu is microalloyed to Fe-Nd-B based amorphous alloys, similar Cu clusters may be formed prior to the crystallization reaction. On this bases, we investigated the effect of Cu and Nb additions on the microstructure and magnetic properties of $Nd_{4.5}Fe_{77}B_{18.5}$ alloy, and found that combined addition of Cu and Nb is very effective in refining the $Fe_3B/Nd_2Fe_{14}B$ nanocomposite produced by crystallization of the amorphous alloy [6,7].

α-Fe/$Nd_2Fe_{14}B$ nanocomposites show higher coercivity than $Fe_3B/Nd_2Fe_{14}B$, thus it is worth exploring the effect of Cu and Nb additions to α-Fe/$Nd_2Fe_{14}B$ nanocomposites as well. One shortcoming of the α-Fe/$Nd_2Fe_{14}B$ system is the difficulty in controlling the microstructure. This is because the glass forming ability of the alloy within the composition range that produce α-Fe/$Nd_2Fe_{14}B$ nanocomposites is very poor. Because of this, the production of α-Fe/$Nd_2Fe_{14}B$ nanocomposite materials in an industrial scale with good reproducibility is challenging. There are a few investigations that reported the beneficial effect of Cu addition to α-Fe/$Nd_2Fe_{14}B$ nanocomposites [8,9], but no work has clarified the role of Cu in the formation of α-Fe/$Nd_2Fe_{14}B$ nanocomposite microstructures due to the limitation of experimental techniques. The optimized hard magnetic properties of α-Fe/$Nd_2Fe_{14}B$ nanocomposites are commonly obtained by partially crystallizing the melt-spun ribbon during solidification. The hard magnetic properties obtained after annealing the melt-spun ribbon is very sensitive to the cooling rate of the melt-spinning; thus reproducibility of the hard magnetic properties obtained from α-Fe/$Nd_2Fe_{14}B$ is not as good as that of $Fe_3B/Nd_2Fe_{14}B$. If optimized nanocomposite microstructure can be processed by crystallizing an amorphous precursor, the reproducibility of the magnetic properties obtained from the α-Fe/$Nd_2Fe_{14}B$ nanocomposites should be significantly improved. For this purpose, we prepared amorphous phase

Table 1 Alloy compositions, heat treatment conditions , constituent phases and magnetic properties of the specimens.

Alloy Composition	Heat Treatment	Constituent Phases	B_r (T)	H_c (kA/m)	$(BH)_{max}$ (kJ/m^3)
$Nd_{4.5}Fe_{77}B_{18.5}$	680°C 10 min	Fe_3B, $Nd_2Fe_{14}B$	1.1	213	57
$Nd_{4.5}Fe_{76.8}B_{18.5}Cu_{0.2}$	660°C 10 min	Fe_3B, $Nd_2Fe_{14}B$	1.2	280	100
$Nd_{4.5}Fe_{75.8}B_{18.5}Nb_1Cu_{0.2}$	660°C 6 min	Fe_3B, $Fe_{23}B_6$, $Nd_2Fe_{14}B$	1.25	287	125
$Nd_8Fe_{87}B_5$	760°C 2 min	α-Fe, $Nd_2Fe_{14}B$	1.02	371	89
$Nd_8Fe_{86}B_5Nb_1$	760°C 2 min	α-Fe, $Nd_2Fe_{14}B$	0.88	361	81
$Nd_8Fe_{85}B_5Nb_1Cu_1$	as-spun 20 m/s	α-Fe, $Fe_{23}B_6$, $Nd_2Fe_{14}B$	0.95	283	76

from alloys based on a composition of $Nd_8Fe_{87}B_5$, and studied the effect of Nb and Cu additions to the microstructures and magnetic properties of α-Fe/$Nd_8Fe_{87}B_5$ nanocomposites.

Experimental

Alloy ingots of the compositions shown in Table 1 were prepared by arc melting $Nd_{4.5}Fe_{77}B_{18.5}$ and $Nd_8Fe_{87}B_5$ mother alloy ingots with small amounts of Cu and Nb. These alloy ingots were melt-spun onto a Cu roll at surface wheel velocities ranging from 20 m/s to 37 m/s in an argon atmosphere. The thickness of the ribbon specimen was approximately 20 μm and the width was approximately 2 mm. The as-melt-spun ribbons were all confirmed to be in the amorphous state by TEM and x-ray diffraction. Thin foil specimens for TEM observations were prepared by ion milling from both sides of the ribbon. Conventional TEM observations were carried out by a Philips CM200 electron microscope. Specimens for atom probe analysis were prepared by mechanically grinding a ribbon to a square rod of approximately 20 mm × 20 mm × 6 mm followed by micro-electropolishing to a sharp needle shape specimen. These specimens were observed by field ion microscope (FIM) and then analyzed by a three dimensional atom probe (3DAP). The 3DAP was equipped with CAMECA tomographic atom probe (TAP) detection system [9] which was installed to a locally designed FIM chamber. The atom probe analyses were performed with a pulse fraction (V_p/V_{dc}) of 0.2 and a pulse repetition rate of 600 Hz at a specimen temperature of 35 K under an ultrahigh vacuum of ~1x10^{-8} Pa.

Cu and Nb Effect on $Fe_3B/Nd_2Fe_{14}B$ Nanocomposite Microstructure

Figures 1 (a) - (d) show bright field TEM micrographs of $Nd_{4.5}Fe_{77}B_{18.5}$, $Nd_{4.5}Fe_{76.8}B_{18.5}Cu_{0.2}$, $Nd_{4.5}Fe_{75.8}B_{18.5}Nb_1Cu_{0.2}$ and $Nd_{4.5}Fe_{76}B_{18.5}Nb_1$ alloys annealed at 660°C for 10 min, respectively [7]. The average grain size of the ternary alloy is approximately 30 nm, while those of the Cu containing quaternary and Cu and Nb containing quinery alloy are approximately 17 nm and 12 nm, re-

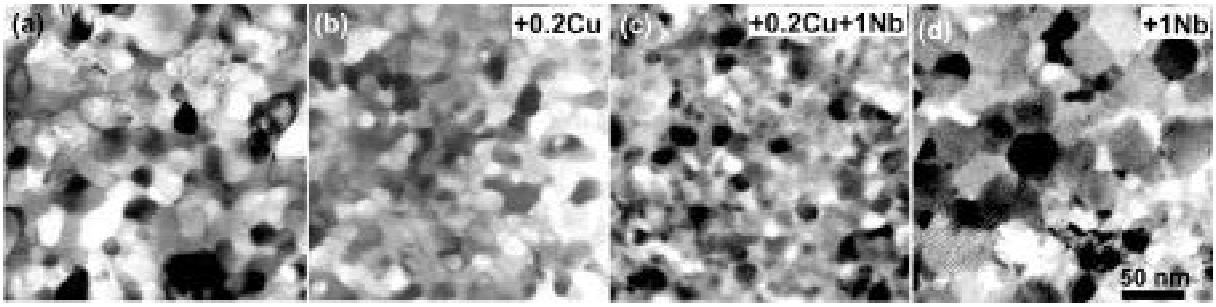

Fig. 1 TEM bright field micrographs of (a) $Nd_{4.5}Fe_{77}B_{18.5}$, (b) $Nd_{4.5}Fe_{76.8}B_{18.5}Cu_{0.2}$, (c) $Nd_{4.5}Fe_{75.8}B_{18.5}Nb_1Cu_{0.2}$ and (d) $Nd_{4.5}Fe_{76}B_{18.5}Nb_1$ alloys. Average grain size is about 30, 17, 12 and 43 nm, respectively.

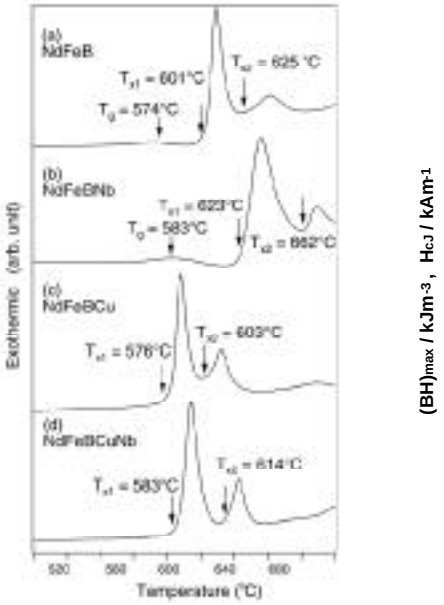

Fig. 2 DSC traces of melt-spun (a) $Nd_{4.5}Fe_{77}B_{18.5}$, (b) $Nd_{4.5}Fe_{76}B_{18.5}Nb_1$, (c) $Nd_{4.5}Fe_{76.8}B_{18.5}Cu_{0.2}$ and (d) $Nd_{4.5}Fe_{75.8}B_{18.5}Nb_1Cu_{0.2}$ ribbons scanned at a heating rate of 20°C/min.

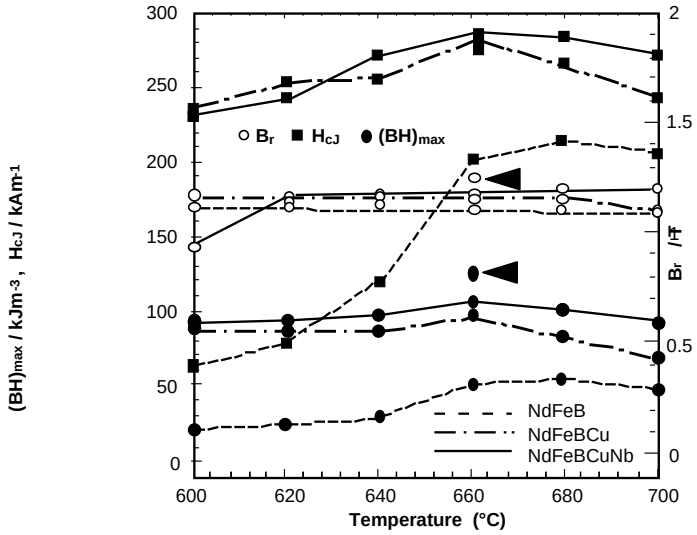

Fig. 3 H_{cJ}, B_r and $(BH)_{max}$ of $Nd_{4.5}Fe_{77}B_{18.5}$, $Nd_{4.5}Fe_{76.8}B_{18.5}Cu_{0.2}$, $Nd_{4.5}Fe_{75.8}B_{18.5}Nb_1Cu_{0.2}$ melt-spun ribbons annealed for 10 min at various temperatures. The arrowheads show the best properties obtained by annealing the quinery alloy for 6 min at 660°C.

spectively. On the other hand, the grain size of the Nb containing quaternay alloy (~50 nm) is larger than that of the ternary alloy. It should be noted that adding only 0.2 atomic percent of Cu to the ternary alloy is effective to reduce the grain size of the optimum nanocomposite microstructure. The microstructure is composed of Fe_3B and $Nd_2Fe_{14}B$ grains in the ternary and quaternary alloys, and there is no change in the constituent phases in these two alloys. Figure 2 shows DSC traces of these four amorphous alloys measured at a heating rate of 20°C/min. The first exothermic peak is attributed to the primary crystallization of Fe_3B from amorphous, and the second peak corresponds to the crystallization of the remaining amorphous phase to $Nd_2Fe_{14}B$. Cu addition reduces the first crystallization temperature by approximately 20°C, suggesting that the Cu addition affects the kinetics of crystallization without changing the phase equilibrium. Single addition of Nb stabilize the amorphous phase, increasing the crystallization temperature by about 20°C. However, the kinetics enhancement effect of Cu is still effective even if Nb is added to the Cu containing alloy. The addition of Nb changes the constituent phases, and $Fe_{23}B_6$ phase was formed in addition to Fe_3B, $Nd_2Fe_{14}B$ in the quinery alloy, thus Nb addition affects the phase equilibrium [7].

Figure 3 shows magnetic properties of the $Nd_{4.5}Fe_{77}B_{18.5}$, $Nd_{4.5}Fe_{76.8}B_{18.5}Cu_{0.2}$ and $Nd_{4.5}Fe_{75.8}B_{18.5}Nb_1Cu_{0.2}$ melt-spun ribbons which were annealed for 10 min at various temperatures. The overall magnetic properties of the quaternary and quinery alloys are significantly improved compared with those of the ternary alloy. The addition of Cu not only improves H_{cJ} and $(BH)_{max}$, but also extends the temperature range to obtain the optimum magnetic properties. In the ternary alloy, the specimen has to be annealed at the temperature range between 660 and 700°C, but the magnetic properties of the Cu containing alloys can be optimized by annealing at a wider temperature range between 600 and 700°C. Further addition of Nb is effective in increasing H_{cJ} and $(BH)_{max}$, although the magnitude of the improvement is small. The best magnetic properties of H_{cJ} = 273 kA/m, B_r = 1.25 T and $(BH)_{max}$ = 125 kJ/m^3 were obtained after annealing the quinery alloy for 6 min at 660°C as indicated by the arrowheads in Fig. 3.

In order to understand the role of Cu atoms during the nucleation and growth stage of the primary Fe_3B crystals, the specimens crystallized at 530°C for 10 min has been studied by 3DAP [6]. Figure 4 (a) shows a 3DAP elemental map of Cu within an analyzed volume of ~14 × 14 × 45 nm. It is apparent that Cu atoms form clusters at this stage with a density of about 10^{24} m^{-3}. The size of the Cu clusters is around 2 nm. In order to evaluate the local concentration change near the cluster more quantitatively, compositional profiles determined from the selected volume are shown in Fig.

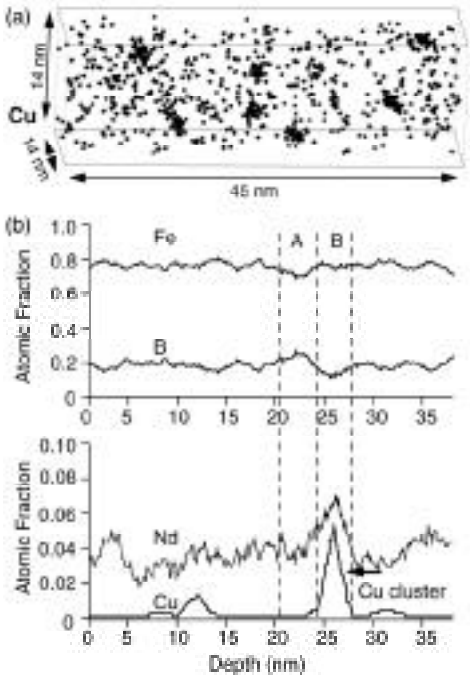

Fig. 4 (a) 3DAP Cu mapping in $Nd_{4.5}Fe_{76.8}B_{18.5}Cu_{0.2}$ alloy annealed at 530°C for 10 min. (b) Concentration depth profiles of Fe, B, Nd and Cu determined from a selected volume in (a).

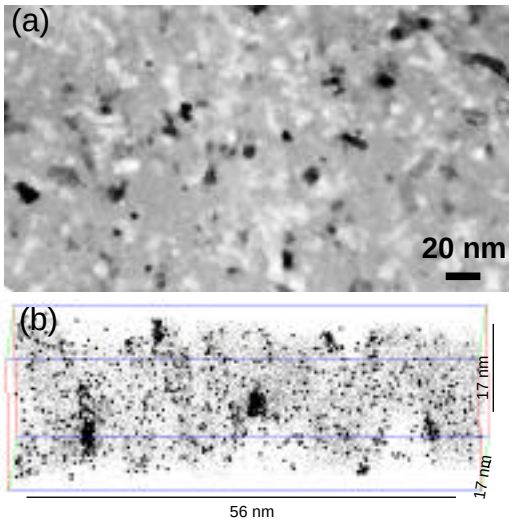

Fig. 5 (a) TEM bright field micrograph showin ga high number density of Fe_3B particles precipitate out of the amrophous matrix of $Nd_{4.5}Fe_{76.8}B_{18.5}Cu_{0.2}$ alloy after annealing at 530°C for 30 min; (b) 3DAP elemental map of Cu and Nd. Cu and Nd atoms are represented by large and small black dots, respectively.

4 (b). The Cu concentration in the Cu cluster is estimated to be around 5.0 at.%. In the Cu-enriched regions, the Nd concentration is approximately 7.0 at.%, which is slightly higher than that in the amorphous phase (4.5 at.%). The concentration of Nd and Cu in these regions is much lower than that of any known Nd-Cu compounds, thus we believe that they do not correspond to any Nd-Cu compounds. The concentrations of Fe and B around the Cu clusters are slightly different from the other region. In Fig. 4 (b), region A adjacent to the Cu enriched region is enriched in B and depleted in Fe than the average values. This is probably because Fe_3B phase is present in region A, suggesting that the Cu clusters act as heterogeneous nucleation sites for the Fe_3B particles.

Figure 5 (a) shows a TEM bright field micrograph of the alloy annealed at 530°C for 30 min. The crystalline particles observed in this micrograph are all Fe_3B (bct structure) embedded in the amorphous matrix, and the second stage crystallization of the $Nd_2Fe_{14}B$ phase does not occur yet in this stage. Figure 5 (b) shows a 3DAP elemental map of Cu and Nd in an analysis volume of approximately ~17 × 17 × 56 nm, where small and large black spots correspond to Nd and Cu atoms, respectively. Fe_3B particles can be easily recognized based on the atomic distribution of Nd because the Nd atoms are fully rejected from the Fe_3B phase. From Fig. 5 (b), it can be clearly seen that each Cu cluster is located at the interface between Fe_3B crystals and the amorphous matrix in direct contact with the Fe_3B particles. Cu atoms are found to be rejected from the Fe_3B particles, so the Cu cluster is located at the amorphous phase side. This result suggests that Cu-enriched regions (or clusters) serve as heterogeneous nucleation sites for the Fe_3B primary crystals.

Several 3DAP data have demonstrated that one Cu cluster is present corresponding to each Fe_3B crystal. This strongly suggests that Fe_3B nanocrystals nucleate at the site of Cu clusters. The reason why Cu clusters serve as heterogeneous nucleation sites for Fe_3B would be explained as follows. From Fig. 4 (b), it can be seen that Nd is also enriched in the Cu cluster region, but the total atomic fraction of Cu and Nd in the cluster is less than 15%. Thus, it is not likely that they are any Nd-Cu compounds with a distinct structure, but they are believed to be still amorphous. So it is unlikely

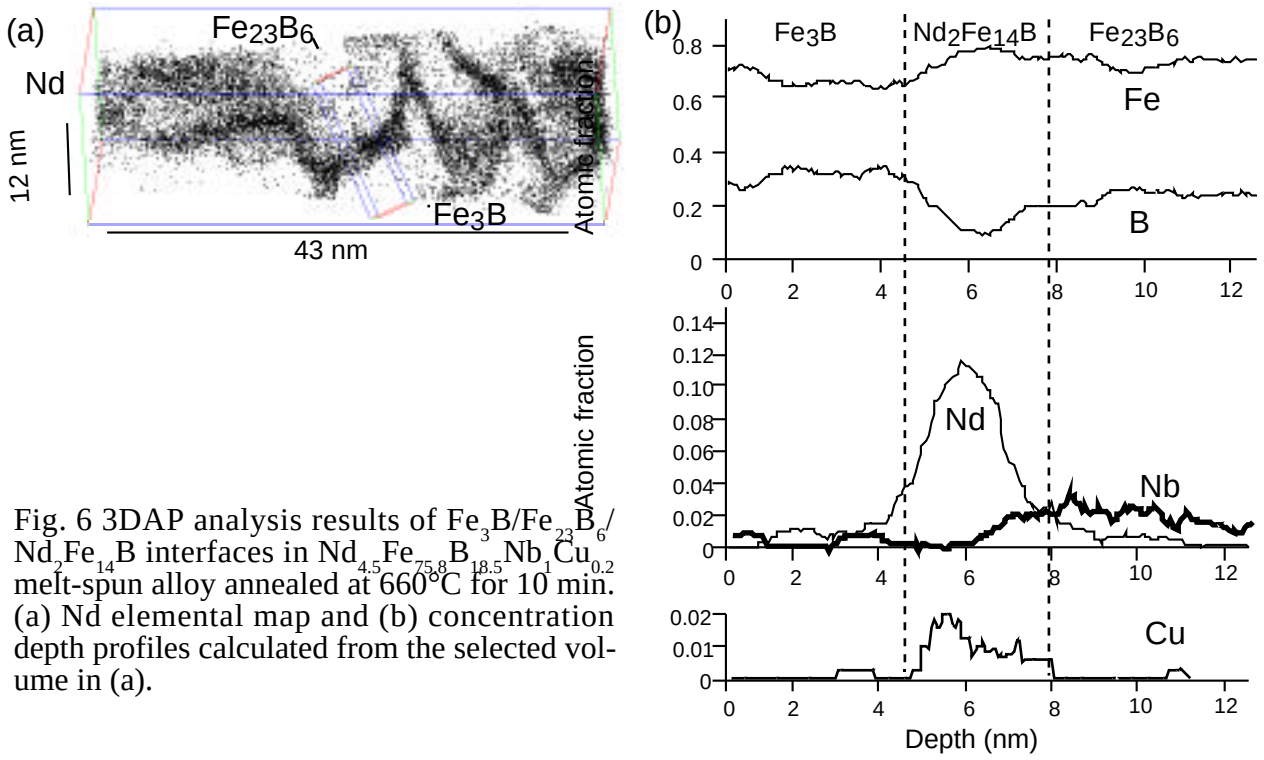

Fig. 6 3DAP analysis results of $Fe_3B/Fe_{23}B_6/Nd_2Fe_{14}B$ interfaces in $Nd_{4.5}Fe_{75.8}B_{18.5}Nb_1Cu_{0.2}$ melt-spun alloy annealed at 660°C for 10 min. (a) Nd elemental map and (b) concentration depth profiles calculated from the selected volume in (a).

that the Cu clusters provide structural heterogeneous nucleation sites for Fe_3B crystals. Rather, the nucleation of the Fe_3B primary crystals would be triggered by a chemical factor. As shown in the atom probe results of Fig. 4 (b), boron atoms pile up at the Cu/amorphous interface (region A) when Cu clusters form. For the formation of Fe_3B crystals, Fe atoms do not have to diffuse much because the matrix Fe composition (76.8 at.%) is very close to the concentration of Fe in the Fe_3B phase, but B atoms have to diffuse in by rejecting Nd atoms. Since Nd has strong affinity with Cu (large negative enthalpy of mixing), when Cu atoms aggregate, Nd atoms are attracted to the Cu atoms, resulting in co-segregation of Cu and Nd. As a result, enrichment of B and depletion of Nd occur at the Cu/amorphous interface, which benefit for the formation of Fe_3B phase adjacent to the Cu clusters.

Combined addition of Cu and Nb further reduces the grain size. 3DAP analysis results showed that the Cu clusters that form in the early crystallization stage trigger the nucleation of the Fe_3B primary particles in the $Nd_{4.5}Fe_{75.8}B_{18.5}Nb_1Cu_{0.2}$ alloy as well. Nb is rejected from the Fe_3B primary particles and partitioned in the remaining amorphous phase. When the remaining amorphous phase crystallizes, $Nd_2Fe_{14}B$ and $Fe_{23}B_6$ phases are formed in the quinery alloy, and Nb is exclusively partitioned in the $Fe_{23}B_6$ phase. The $Fe_{23}B_6$ phase is not observed in the ternary and quaternary alloy, hence it is concluded that Nb addition induces the formation of the $Fe_{23}B_6$ phase in the second stage of the crystallization. The 3DAP analysis result of the final microstructure of the $Nd_{4.5}Fe_{75.8}B_{18.5}Nb_1Cu_{0.2}$ alloy is shown in Fig 6. Fe_3B, $Fe_{23}B_6$ and $Nd_2Fe_{14}B$ are observed in the analysis volume. Cu is partitioned in the $Nd_2Fe_{14}B$ phase, whereas Nb is exclusively partitioned in the $Fe_{23}B_6$ phase.

Cu and Nb Effect on α-Fe/$Nd_2Fe_{14}B$ Nanocomposite Microstructure

Figure 7 shows x-ray diffraction results of the $Nd_8Fe_{85}B_5Nb_1Cu_1$ and $Nd_8Fe_{86}B_5Nb_1$ ribbons melt-spun at wheel surface velocities of 35 and 37 m/s, respectively. The amorphous feature of these as-melt-spun ribbons was also confirmed by transmission electron microscopy observations. However, crystalline phases always appeared in the case of ternary $Nd_8Fe_{87}B_5$ alloy even at a wheel surface velocity of 40 m/s. This suggests that Nb addition improves the glass forming ability of $Nd_8Fe_{87}B_5$ alloy. Differential scanning calorimetric (DSC) curves measured from $Nd_8Fe_{85}B_5Nb_1Cu_1$ and $Nd_8Fe_{86}B_5Nb_1$ amorphous alloys show only one exothermic peak as shown in Fig. 8, suggesting that the crystallization occurs in one stage. The peak temperature of the Cu-containing alloy is

lower than that of Cu-free alloy by about 30°C, suggesting that Cu enhances the crystallization kinetics in this case as well. One exothermic peak means that the crystallization occurs at one time. In this kind of alloys, the microstructure mainly contains two crystalline phases, α-Fe and $Nd_2Fe_{14}B$. The above DSC results suggest that the two phases precipitate at the same time, so the crystallization mode is probably of eutectic type.

3DAP results obtained from the as-quenched $Nd_8Fe_{85}B_5Nb_1Cu_1$ amorphous alloy showed that the solute atoms are uniformly distributed (the data is not shown here). In order to investigate how solute redistribution occurs by annealing, the as-quenched specimen was annealed at a temperature well below the crystallization temperature and the solute distribution was observed by 3DAP. Figure 9 shows HREM image with inset corresponding selected area electron diffraction (SAED) pattern of the $Nd_8Fe_{85}B_5Nb_1Cu_1$ alloy annealed at 495°C for 30 min. This annealing condition was chosen based on the DSC result so that crystallization does not occur. At this stage, one can see that the overall microstructure is still amorphous, although some fringes corresponding to α-Fe are visible. In addition to the major amorphous halo ring, SAED ring patterns corresponding to α-Fe (110), (200) and (211) are also observed. Figure 10 (a) is 3DAP elemental mapping of Cu atoms in a volume of ~17 × 17 × 60 nm^3 obtained from this specimen. It is apparent that Cu atoms form clusters at this stage with a density of about 10^{24} m^{-3}. The size of the Cu clusters is around 3 nm. The concentration in Cu clusters is calculated to be about 13 at.% as shown in the composition profiles (Fig. 10 (b)) calculated from the selected volume of 3 × 3 × 15 nm^3 in Fig. 10 (a). At this stage, all the other solute elements are almost uniformly distribute in the alloy.

Figures 11 show bright field TEM micrographs of (a) $Nd_8Fe_{85}B_5Nb_1Cu_1$ and (b) $Nd_8Fe_{86}B_5Nb_1$ alloys annealed at 760°C for 2 min and (c) $Nd_8Fe_{87}B_5$ alloy melt-spun at a wheel surface velocity of 20m/s. There is not much difference in the grain size between the $Nd_8Fe_{85}B_5Nb_1Cu_1$ and $Nd_8Fe_{86}B_5Nb_1$ alloys that were crystallized from an amorphous phase. Microdiffraction investigations confirmed that the larger grains are $Nd_2Fe_{14}B$ phase, whose grain size is about 50 nm; small grains are α-Fe, whose grain size is about 20 nm. But in the $Nd_8Fe_{85}B_5Nb_1Cu_1$ sample, some of the smaller grains were identified as $Fe_{23}B_6$. On the other hand, the as-quenched ternary alloy has much finer microstructure, α-Fe≈15nm and $Nd_2Fe_{14}B$≈35nm, as shown in Fig. 11 (c). Apparently, the grain sizes of α-Fe and $Nd_2Fe_{14}B$ phases are much larger than the optimum values that was predicted by modeling calculation by Fischer *et al.* [12], where the most suitable sizes of α-Fe and $Nd_2Fe_{14}B$ are predicted to be 10 nm and 20 nm, respectively.

In the $Nd_8Fe_{85}B_5Nb_1Cu_1$ amorphous alloy, the Cu atoms do form high density of clusters (size is about 3 nm and the Cu concentration is around 13 at.%) prior to the crystallization reaction, as

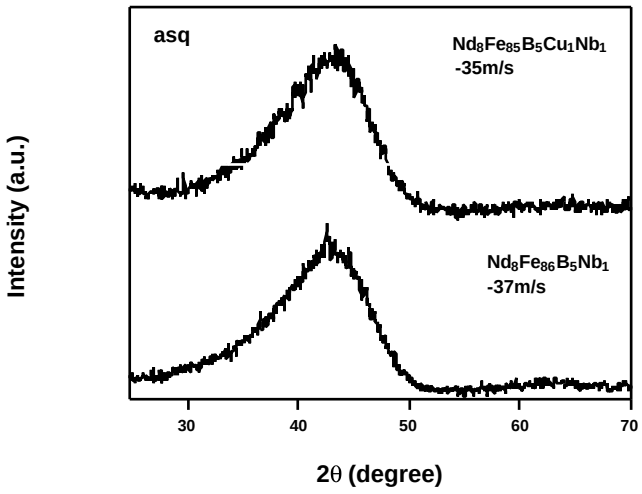

Fig. 7 XRD results of $Nd_8Fe_{85}Nb_1Cu_1$ and $Nd_8Fe_{86}B_5Nb_1$ alloys melt-spun at wheel surface velocity of 35 m/s and 37 m/s, respectively.

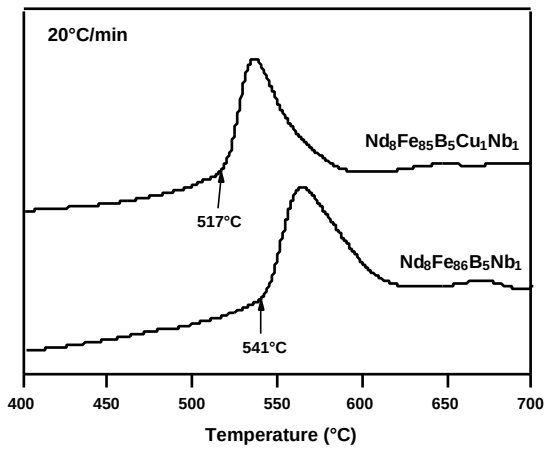

Fig. 8 DSC traces of as-quenched $Nd_8Fe_{85}Nb_1Cu_1$ and $Nd_8Fe_{86}B_5Nb_1$ amorphous alloys.

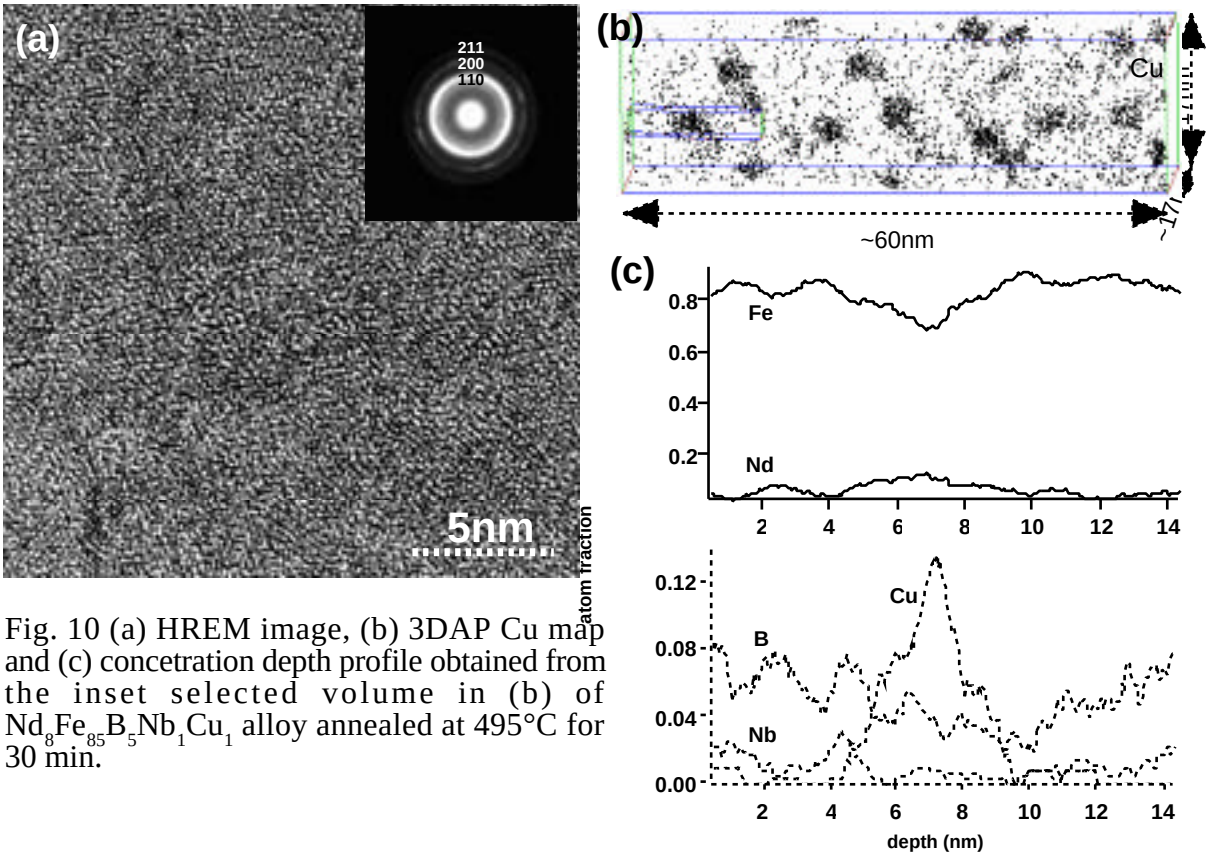

Fig. 10 (a) HREM image, (b) 3DAP Cu map and (c) concetration depth profile obtained from the inset selected volume in (b) of $Nd_8Fe_{85}B_5Nb_1Cu_1$ alloy annealed at 495°C for 30 min.

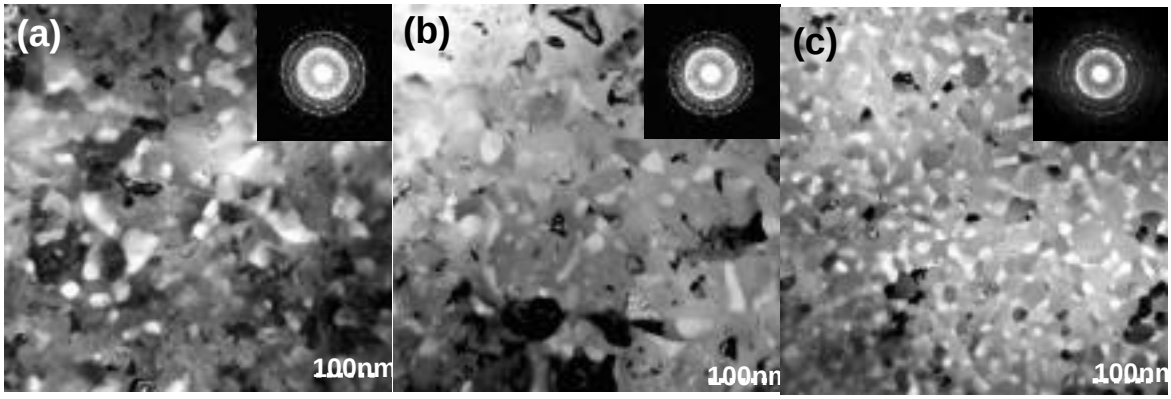

Fig. 11 TEM bright field images and corresponding SAED patterns of (a) $Nd_8Fe_{85}B_5Nb_1Cu_1$, (b) $Nd_8Fe_{86}B_5Nb_1$ alloys annealed at 760°C for 2 min, and (c) as-quenched $Nd_8Fe_{87}B_5$ alloy melt-spun at a wheel surface velocity of 20 m/s.

shown in Fig. 10 (b), but those clusters do not appear to serve as heterogeneous nucleation sites for α-Fe particles. This result is in contrast to the case of $Nd_{4.5}Fe_{76.8}B_{18.5}Cu_{0.2}$ amorphous alloy, in which Cu clusters serve as heterogeneous nucleation sites for Fe_3B primary crystals, thereby refining the $Fe_3B/Nd_2Fe_{14}B$ nanocomposite microstructure [3, 5]. In order for Cu clusters to serve as heterogeneous nucleation sites for a-Fe particles, Cu clusters may need to develop to fcc-Cu as was observed in Fe-Si-B-Nb-Cu [2]. It is known that $\{111\}_{Cu}$ and $\{011\}_{Fe}$ have very good lattice matching, thus $\{111\}_{Cu}$ would provide low interfacial energy if α-Fe particle is nucleated on this interface. Based on the present 3DAP data, the Cu concentration in the Cu clusters observed in $Nd_8Fe_{85}B_5Nb_1Cu_1$ amorphous alloy is only around 13 at.%, and HREM observations do not show that there is any fcc-Cu crystallite in the amorphous matrix. Therefore, the structural feature of the Cu clusters is limited only in the short range, and they do not grow to have a distinct feature as the

fcc structure. This may be the reason why the Cu clusters do not work as heterogeneous nucleation sites for α-Fe particles during the crystallization of the $Nd_8Fe_{85}B_5Nb_1Cu_1$ amorphous alloy. Thus, the formation of Cu clusters does not make any beneficial effect on the microstructural evolution of α-Fe/$Nd_2Fe_{14}B$ nanocomposites. Hence, as can be seen from Fig. 11 (a) and (b), there is no significant difference in grain size between the Cu-containing and Cu-free alloys.

The present authors recently investigated the microstructural evolution in $Nd_8Fe_{76.5}B_6Co_8Nb_1Cu_{0.5}$ and $Nd_8Fe_{77}Co_8B_6Nb_1$ alloys that form α-Fe/$Nd_2Fe_{14}B$/amorphous nanocomposites [9]. In these alloys, 3DAP analyses results revealed that Nb atoms strongly segregate in the intergranular remaining amorphous phase, which stabilizes the remaining amorphous phase and control the grain growth during melt-spinning and post-annealing. Hence, it was concluded that Nb atoms play a critical role in controlling the α-Fe/$Nd_2Fe_{14}B$ nanocomposite microstructure in the $Nd_8Fe_{77}Co_8B_6Nb_1$ alloy. However, the present result has shown that Nb is not effective in refining the α-Fe/$Nd_2Fe_{14}B$ nanocomposite microstructure that are produced by crystallizing the amorphous phase, although it does improve the glass forming ability of the alloy. The finest microstructure was observed in the as-melt-spun specimen of ternary $Nd_8Fe_{87}B_5$ alloy. In the final microstructure, Nb is partitioned in $Fe_{23}B_6$ phase, and it does not give any beneficial effect in refining the microstructure.

Summary

The nanocrystallization processes in Nd-Fe-B amorphous alloys microalloyed with Cu and Nb have been studied by TEM and 3DAP. In both $Nd_{4.5}Fe_{77}B_{18.5}$ and $Nd_8Fe_{87}B_5$ amorphous alloys, Cu form a high density of clusters in the early stage of annealing. The number density of these clusters are in the order of 10^{24} m^{-3}, and these serve as heterogeneous nucleation sites for the Fe_3B primary crystals in $Nd_{4.5}Fe_{76.8}B_{18.5}Cu_{0.2}$ and $Nd_{4.5}Fe_{75.8}B_{18.5}Nb_1Cu_{0.2}$ alloys. In these alloys, Cu and Nd cosegregate in the early stage of annealing, which chemically trigger heterogeneous nucleation of the Fe_3B primary particles. When the remaining amorphous phase crystallizes to the $Nd_2Fe_{14}B$ phase, the Cu clusters completely dissolve in this phase. Nb atoms induce formation of $Fe_{23}B_6$ soft magnetic phase during the second stage crystallization of the $Nd_{4.5}Fe_{75.8}B_{18.5}Nb_1Cu_{0.2}$ alloy. On the other hand, Cu clusters formed in $Nd_8Fe_{86}B_5Nb_1Cu_1$ alloys does not serve as heterogeneous nucleation sites for α-Fe, thus Cu addition is not beneficial for reducing the grain size of the α-Fe/$Nd_2Fe_{14}B$ nanocomposite magnet. Cu additions are effective only in the alloy system that form Fe_3B/$Nd_2Fe_{14}B$ nanocomposites.

References

[1] S. Hirosawa, H. Kanekiyo, and M. Uehara, J. Appl. Phys. **73** (1993) 6488.
[2] H. Kanekiyo, M. Uehara, and S. Hirosawa , IEEE Trans. Magn. **29** (1993) 2863.
[3] S. Hirosawa and H. Kanekiyo, Mater. Sci. Eng. A **217** (1996) 367.
[4] Y. Yoshizawa and K. Yamauchi, Mater. Trans. JIM, **31** (1990) 307.
[5] K. Hono, D. H. Ping, M. Ohnuma and H. Onodera, Acta mater. **47** (1999) 997.
[6] D. H. Ping, K. Hono, H. Kanekiyo and S. Hirosawa, J. Appl. Phys. **85**, p. 2448 (1999).
[7] D. H. Ping, K. Hono, H. Kanekiyo and S. Hirosawa, Acta mater. **47** (1999) 4641.
[8] H. Chiriac and M. Marinescu, J. Appl. Phys. **83** (1998), 6628.
[9] M. Hamano, M. Yamasaki, H. Mizuguchi, H. Yamamoto and A. Inoue in Rare-Earth Magnets and their Applications, vol. 1, Proc. 5th Inter. Workshop on Rare-Earth Magnets and their applications, eds by L. Schultz and K. H. Müller, Werkstoff-Informationsgesellschaft, Germany, 1998, pp. 199.
[10] D. Blavette, B. Deconihout, A. Bostel, J. M. Sarrau, M. Bouet, and A. Menand, Rev. Sci. Instrum. **64**, p. 2911 (1993).
[11] R. Fischer, T. Schrefl, H. Kronmüller and J. Fidler, J. Magn. Magn. Mater. **153** (1996), 35.
[12] Y. Q. Wu, D. H. Ping, K. Hono, M. Hamano and A. Inoue, J. Appl. Phys. **87** (2000), in press.